

## Original article

# Interaction of Cu-Al melts with $\text{Cr}_2\text{AlC}$ and $(\text{Cr}_{0.95}\text{Mn}_{0.05})_2\text{AlC}$ MAX-phases

Sergei Zhevnenko<sup>✉\*</sup>, Mikhail Gorshenkov, Vladimir Gorshkov

Physical Chemistry Department, National University of Science and Technology MISIS, Leninsky pr. 4, Moscow 119049, Russia

### Keywords:

MAX-phases  
 $(\text{Cr}_{0.95}\text{Mn}_{0.05})_2\text{AlC}$   
Cu melt  
capillary phenomena  
composite material

### Cited as:

Zhevnenko, S., Gorshenkov, M., Gorshkov, V. Interaction of Cu-Al melts with  $\text{Cr}_2\text{AlC}$  and  $(\text{Cr}_{0.95}\text{Mn}_{0.05})_2\text{AlC}$  MAX-phases. *Capillarity*, 2025, 15(2): 33-43.  
<https://doi.org/10.46690/capi.2025.05.02>

### Abstract:

New materials based on MAX-phases require methods of soldering, impregnation and knowledge of corrosion resistance to melts at high temperatures. Direct observations of the interaction of melts with MAX-phases provide the most complete information on contact angles, absorption. In our work, high-speed thermal imaging is used, which allows recording thermal effects during the interaction of melts with a solid phase. Melts with aluminum are reactive and dissolve almost all metals. On the other hand, copper allows reducing reactivity by diluting aluminum. This is the reason for choosing copper-aluminum alloys to study corrosion and capillary interaction with the widespread MAX-phases on  $\text{Cr}_2\text{AlC}$  base. The interaction between two-component Al-Cu melts,  $\text{Cr}_2\text{AlC}$  and  $(\text{Cr}_{0.95}\text{Mn}_{0.05})_2\text{AlC}$  was investigated at temperatures reaching  $1,150^\circ\text{C}$  under a vacuum of  $10^{-3}$  Pa. Pure aluminum melt uniformly dissolves MAX-phases at elevated temperatures without wetting it or infiltrating the porous structure. In contrast, interaction with the pure copper melt results in the decomposition of MAX-phases, leading to the formation of a rigid framework composed of chromium carbides, which is impregnated with Cu(Al,Cr) bronze. By adjusting the aluminum content in the copper melt, it is possible to inhibit the complete decomposition of MAX-phases while simultaneously infiltrating and sintering MAX-phases powder to create a mechanically robust composite material.

## 1. Introduction

Over the past two decades, MAX-phases of various compositions have been extensively studied due to their unique combination of metallic and ceramic properties (Barsoum and Radovic, 2011; Li et al., 2014; Sokol et al., 2019; Lei and Lin, 2022). These materials exhibit high thermal stability, excellent electrical conductivity, and outstanding mechanical strength, making them promising for applications under extreme conditions. Particular attention has been paid to  $\text{Cr}_2\text{AlC}$ -based MAX-phases, including those alloyed with manganese and other elements, as they are used in high-temperature corrosion-resistant coatings and as components in composite materials with enhanced wear resistance (Mockute et al., 2013;

Shamsipoor et al., 2020; Tabares et al., 2022). However, their practical application requires the development of reliable joining techniques, such as brazing, welding, or sintering, as well as a thorough understanding of their interaction with metal melts.

Despite the growing interest in MAX-phases, data on their interaction with melts remain limited. Existing studies primarily focus on solid-state reactions (Smialek and Garg, 2015; Li et al., 2020; Zuber et al., 2024), while processes occurring upon contact with liquid metals are poorly understood. This is particularly relevant for copper-based systems, which are widely used in brazing ceramics and metals (Liu et al., 2003; Wang et al., 2024). Previous works, including our own re-

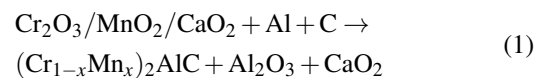
search (Zhevnenko and Gorshenkov, 2022), have shown that a copper melt induces the degradation of  $\text{Cr}_2\text{AlC}$ , leading to the formation of chromium carbides and a bronze matrix. The introduction of manganese slows down this process but does not completely prevent it (Zhevnenko and Gorshenkov, 2024). When exposed to molten Cu,  $\text{Cr}_2\text{AlC}$  demonstrates limited chemical reactivity, as Cu does not form stable carbides or intermetallics with Cr or Al under typical conditions. However, studies indicate that prolonged exposure at elevated temperatures (above 1,100 °C) can lead to partial decomposition of  $\text{Cr}_2\text{AlC}$ , releasing Al into the melt and forming Cu(Al) solid solutions, while the Cr-C framework remains largely intact (Barsoum and El-Raghy, 2001).

The wetting behavior of Cu on  $\text{Cr}_2\text{AlC}$  surfaces is another critical aspect of their interaction. Experimental data show that pure Cu exhibits poor wettability on  $\text{Cr}_2\text{AlC}$ , with contact angles exceeding 90° due to the non-reactive nature of the interface. However, the addition of active elements such as Ti or Cr to the Cu melt can significantly improve wettability by reducing interfacial energy and promoting the formation of interfacial reaction layers. For instance, Ti additions lead to the formation of TiC and Ti-Al intermetallics at the interface, enhancing bonding strength (Zhevnenko and Gorshenkov, 2022). This suggests that alloying Cu with reactive elements is a viable strategy for improving adhesion in Cu/ $\text{Cr}_2\text{AlC}$  composites or joints. At the same time, with partial disintegration of MAX-phases, some of the chromium also dissolves in the copper melt, improving wetting inside the porous MAX-phases. This study investigated the possibility of reducing the chemical potential of aluminum in copper melts by increasing its concentration. The goal was to examine the capillary interaction of Cu-Al melts with  $\text{Cr}_2\text{AlC}$  and  $(\text{Cr}_{0.95}\text{Mn}_{0.05})_2\text{AlC}$  MAX-phases and determine the conditions under which impregnation and powder bonding can occur without degrading MAX-phases. A stepwise heating method was employed to study the interaction dynamics between the melt and a porous substrate, while the resulting phase compositions were analyzed using electron microscopy and energy-dispersive spectroscopy. The findings provide insights into the feasibility of developing stable composites based on MAX-phases and copper alloys. This study demonstrates that the interaction between MAX-phases and copper melts is a complex process dependent on the composition of both MAX-phases and the melt. Increasing the aluminum content in copper may reduce the degradation rate of MAX-phases; however, further research is required to fully prevent its decomposition. The obtained data are crucial for advancing joining technologies for MAX-phases and metals, as well as for designing composite materials with improved performance characteristics.

## 2. Experimental

The fundamental experimental setup for investigating the interaction between the melt and the porous substrate is illustrated in Fig. 1(a). High-purity, dense graphite was used as the material for the dispenser to extrude the melt onto the substrate. All the chamber components, including the heater,

were also made from graphite. Heating was effected by direct electric current, and the temperature of the substrate was monitored using a tungsten-rhenium thermocouple and a thermal imaging camera. The temperature was averaged over the lateral surface area of the substrate. A discrepancy of approximately 10-20 °C was observed between the thermocouple readings and the thermal imaging temperature measurements on the substrate. Video was captured with a high-speed CP70-2-M/C-1,000 camera at frame rates ranging from 500 to 7,000 frames per second, while thermal imaging was performed using an Optris PI 1M camera at a frame rate of 1,000 frames per second or higher. The experiments involved extruding a droplet from the dispenser at a constant temperature under a vacuum of  $10^{-3}$  Pa onto a polished substrate composed of pressed and pre-cleaned powders of  $(\text{Cr}_{0.95}\text{Mn}_{0.05})_2\text{AlC}$  and  $\text{Cr}_2\text{AlC}$ . The vacuum was generated using a diffusion pump equipped with a water-cooled trap, operating in conjunction with a rotary pump. The primary objective of the experiment was to observe the shape and volume of the molten droplet at varying temperatures on substrates of  $(\text{Cr}_{0.95}\text{Mn}_{0.05})_2\text{AlC}$  and  $\text{Cr}_2\text{AlC}$ . Key parameters such as the contact angle, contact diameter, and volume of the deposited droplet were measured. The profile of the pendant and sessile drop was fitted with a DropShape software (Open Science Ltd., Moscow, Russia). The drop profile is a projection of the rotation figure and allows calculating the drop volume. The angles were determined in the program automatically and manually. Variations in the droplet volume provided insight into the dynamics of molten absorption (impregnation). The melts were prepared from 99.99 wt.% pure components by direct melting in a graphite dispenser under vacuum conditions. The melting temperature was maintained below 1,150 °C to prevent significant carbon dissolution in aluminum. At lower temperatures, the melts did not wet graphite within timeframes of tens of minutes (Kennedy et al., 2000; Pittoni et al., 2012; Sarina et al., 2012). In this study, manganese-doped  $(\text{Cr}_{1-x}\text{Mn}_x)_2\text{AlC}$  phases were synthesized via self-propagating high-temperature synthesis. The composition of the initial mixtures was calculated based on the following chemical reaction equation:



where  $x = 0$  and 0.05.

The starting mixtures, composed of chemically pure components, were placed in transparent quartz crucibles with a diameter of 20 mm and a height of 50 mm. Synthesis was conducted in a 3 L self-propagating high-temperature synthesis reactor under an initial argon pressure of  $P_0 = 5$  MPa (Gorshkov et al., 2018; Gorshkov et al., 2021). X-ray phase analysis of the synthesized samples was performed using a Bruker Phaser 2 diffractometer with Cu  $K_\alpha$  radiation and a semiconductor detector. X-ray diffraction patterns were acquired by rotating the sample holder over an angular range of  $2\theta = 10$ -100°. The analysis revealed that for  $x = 0$ , the material consisted primarily of the MAX phase  $\text{Cr}_2\text{AlC}$ , along with residual chromium carbides ( $\text{Cr}_{23}\text{C}_6$ ,  $\text{Cr}_7\text{C}_3$ ) and chromium aluminides ( $\text{CrAl}$ ,  $\text{CrAl}_2$ ). For  $x = 0.05$ , MAX-phases  $(\text{Cr}_{0.95}\text{Mn}_{0.05})_2\text{AlC}$  was identified, with the presence

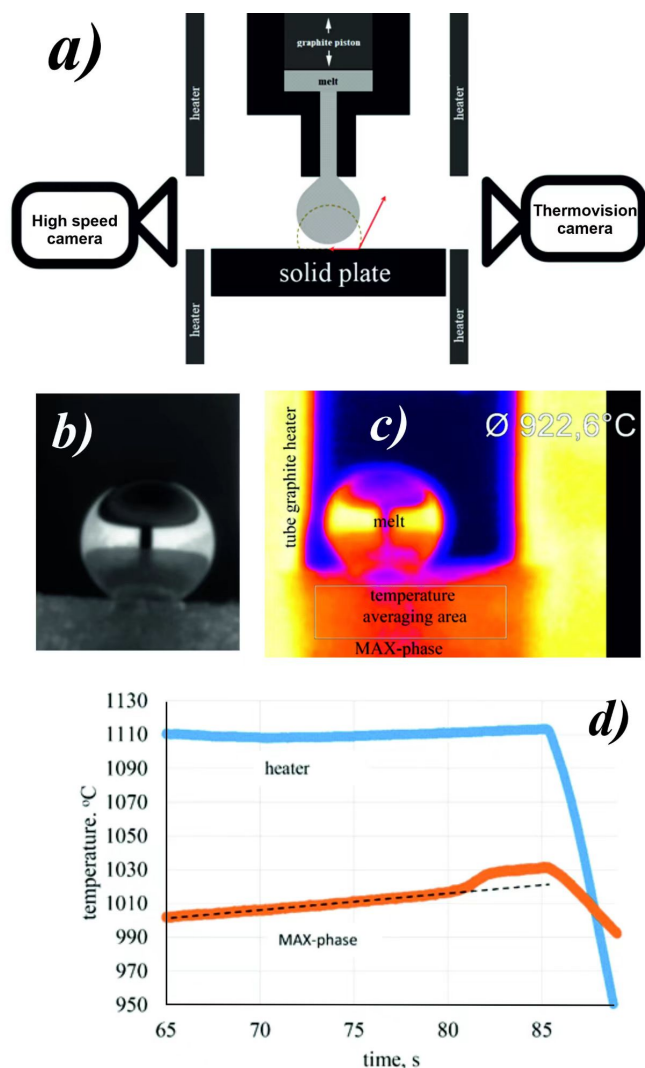


**Fig. 1.** Experimental scheme (a) and view of the melt's drop in the video camera at high temperature lying on MAX-phases ( $\text{Cr}_{0.95}\text{Mn}_{0.05}$ ) $_2\text{AlC}$  (b), view of the drop in the thermal camera is shown in (c). Thermograms of the tubular heater and MAX-phases substrate are presented in (d). The dashed line shows the temperature trend of the substrate until the onset of non-linear temperature change, the point of the curve break is the beginning of cooling.

of chromium aluminide ( $\text{Cr}_5\text{Al}_8$ ). The samples were ground into powder and subsequently treated with a 20% HCl aqueous solution for 24 hours to remove intermetallic phases. In the manganese-doped samples, MAX-phases reflections were shifted relative to those of  $\text{Cr}_2\text{AlC}$ , indicating the substitution of chromium atoms by manganese atoms. The manganese content in MAX-phases was quantified using energy-dispersive X-ray spectrometry following phase purification in hydrochloric acid. The purified MAX-phases powders were pressed at room temperature under a pressure of 25 MPa, and their density was determined through weighing and geometric measurements. For both compositions, the porosity was approximately 20%, and the density of the sintered phases was assumed to be  $5.25 \text{ g/cm}^3$  (Gonzalez-Julian et al., 2016; Zakeri-Shahroudi et al., 2022). Despite the low pressing temperatures and pressures, the samples exhibited sufficient mechanical strength for wetting and impregnation experiments. Furthermore, the

phase state was evaluated by measuring microhardness using a Micromet 5101 instrument under an applied load of 500 mN.

Droplets of the melt were deposited onto the surface of MAX-phases using a graphite dropper. Real-time observations of the droplets were conducted under continuous heating at a rate of approximately  $100 \text{ }^{\circ}\text{C}/\text{min}$ . Heating was terminated when changes in the droplet shape and volume were detected. A representative thermogram is presented in Fig. 1(d). At the heating rate used, the temperature of the heater exceeded that of the substrate, indicating that heating occurred in dynamic mode. Once the droplet either disappeared or reached a stable state, the system was cooled. Notably, an increase in the substrate temperature (exceeding the temperature threshold indicated by the dashed line in Fig. 1(d)) was associated with active chemical interactions. The study utilized melts of pure copper, pure aluminum, and their alloys with compositions of Al+2 at.% Cu, Al+17 at.% Cu, Al+33 at.% Cu, and Cu-17 at.

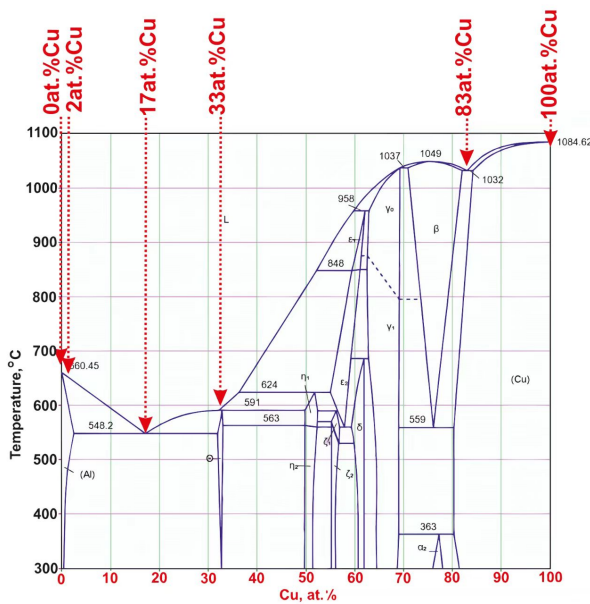


**Fig. 2.** Al-Cu phase diagram with Al-Cu melt concentrations used in experiments (marked by the arrows).

% Al. The corresponding positions of these compositions on the phase equilibrium diagram are illustrated in Fig. 2.

### 3. Results and discussion

#### 3.1 Structural and phase transformations under melt's infiltration

Fig. 3 presents the X-ray diffraction spectra of  $\text{Cr}_2\text{AlC}$  and  $(\text{Cr}_{0.95}\text{Mn}_{0.05})_2\text{AlC}$  powders following purification in hydrochloric acid, subsequent washing with distilled water and alcohol, and drying. The spectra reveal that nearly all prominent diffraction peaks correspond to reflections from MAX-phases. The lattice parameters of MAX-phases in the manganese-doped sample differ from those of the undoped  $\text{Cr}_2\text{AlC}$ , as evidenced by the shift of MAX-phases peaks towards lower diffraction angles. Additionally, the spectra indicate the presence of minor quantities of chromium carbides, specifically  $\text{Cr}_3\text{C}_2$  and  $\text{Cr}_7\text{C}_3$ , in the sample after hydrochloric acid purification. Scanning electron microscopy images of the purified MAX-phases powders are displayed in Figs. 3(b) and 3(c). The micrographs demonstrate that the powder particles are coarse-grained, with sizes ranging from 0.1 to 0.5 mm, and exhibit a plate-like morphology. Some fragments display the characteristic layered structure inherent to MAX-phases, as highlighted in Fig. 3(c). During the compaction of the powder into a bulk sample, some degree of anisotropy is introduced, resulting in the formation of an axial texture due to the plate-like morphology of the original powder particles.

Upon contact with MAX-phases  $(\text{Cr}_{0.95}\text{Mn}_{0.05})_2\text{AlC}$  and  $\text{Cr}_2\text{AlC}$ , the pure copper melt induces the decomposition of MAX-phases, resulting in the formation of a rigid framework of chromium carbides. The interstitial spaces within this framework are filled with copper, which contains dissolved aluminum and chromium, as evidenced by the bright regions observed beneath the droplet in the inset of Fig. 4(a) (Zhev-

nenko and Gorshenkov, 2022). Concurrently, the composition of the droplet on the surface is also altered. This decomposition process occurs at virtually any temperature exceeding the melting point of pure copper. A notable difference in the interaction between the manganese-doped MAX-phases and  $\text{Cr}_2\text{AlC}$  is the larger contact angle (exceeding  $100^\circ$ ) of the copper melt on the surface of the manganese-doped sample (Zhevnenko and Gorshenkov, 2024). Furthermore, the decomposition process propagates radially from the contact surface, despite the relatively weak adhesion of the droplet to the substrate. In experiments with aluminum-copper melts, the initial angles were very large,  $130\text{--}150^\circ$ . This indicates that the surface is oxidized. As the droplet is absorbed and its volume decreases, the angle decreases due to the fixation of the triple equilibrium line (vacuum-liquid-solid) and indicates a large hysteresis of the contact angle.

When in contact with pure aluminum (Fig. 4(b)), MAX-phases undergoes dissolution, and at temperatures of  $1,030^\circ\text{C}$  and above, this process occurs at a significant rate. The molten droplet becomes saturated with chromium and carbon, leading to the formation of aluminum carbide both at the contact surface and within the droplet itself, as indicated by the dark plate-like regions in the inset of Fig. 4(b). Upon cooling, the sample exhibits no mechanical strength and disintegrates rapidly under minimal load, indicating that no effective powder bonding occurs. The addition of copper to aluminum, even in small quantities (a few atomic percent), significantly alters the nature of the interaction. In this case, the porous MAX-phases plate retains considerably greater mechanical strength after contact with the melt. This suggests the formation of liquid layers between the powder particles at distances far from the contact surface, which act to bond individual particles, although these layers are not detectable by scanning electron microscopy. Near the contact surface, a portion of MAX-phases decomposes to form chromium carbides, as evidenced by the light regions in Fig. 5(a). Notably, no aluminum carbide is observed in the region of MAX-phases under these conditions.

Increasing the copper concentration in the aluminum melt (Figs. 5(b), 5(c), and 5(d)) results in the expansion of the interlayers between the grains of  $(\text{Cr}_{0.95}\text{Mn}_{0.05})_2\text{AlC}$ . These interlayers are formed from aluminum melts containing chromium (up to 20 wt.% Cr) and copper. The copper-based melt also appears at considerable distances from the contact surface, as indicated by the brightest regions in Fig. 5(c). Within the droplet, the formation of  $\text{Al}_4\text{C}_3$  (visible as black areas in Fig. 5(d)),  $\text{Al}(\text{Cr})$  solid solutions, and  $\text{Cu}(\text{Al})$  alloys is observed. Notably,  $\text{Al}_4\text{C}_3$ , which is prone to degradation in moisture-containing environments, is also formed within the compacted phase, specifically in the spaces between the powder particles. The compacted MAX-phases powders gain mechanical strength due to the formation of wetting melts based on  $\text{Al}(\text{Cr})$  distributed throughout the sample volume (with characteristic dimensions of  $10 \times 5 \times 5 \text{ mm}^3$ ). During the interaction of pure copper melt with  $\text{Cr}_2\text{AlC}$  and  $(\text{Cr}_{0.95}\text{Mn}_{0.05})_2\text{AlC}$ , the formation of the melt inside the material occurs simultaneously with the decomposition of these phases and the dissolution of aluminum in the melt (Zhevnenko and Gorshenkov, 2022;

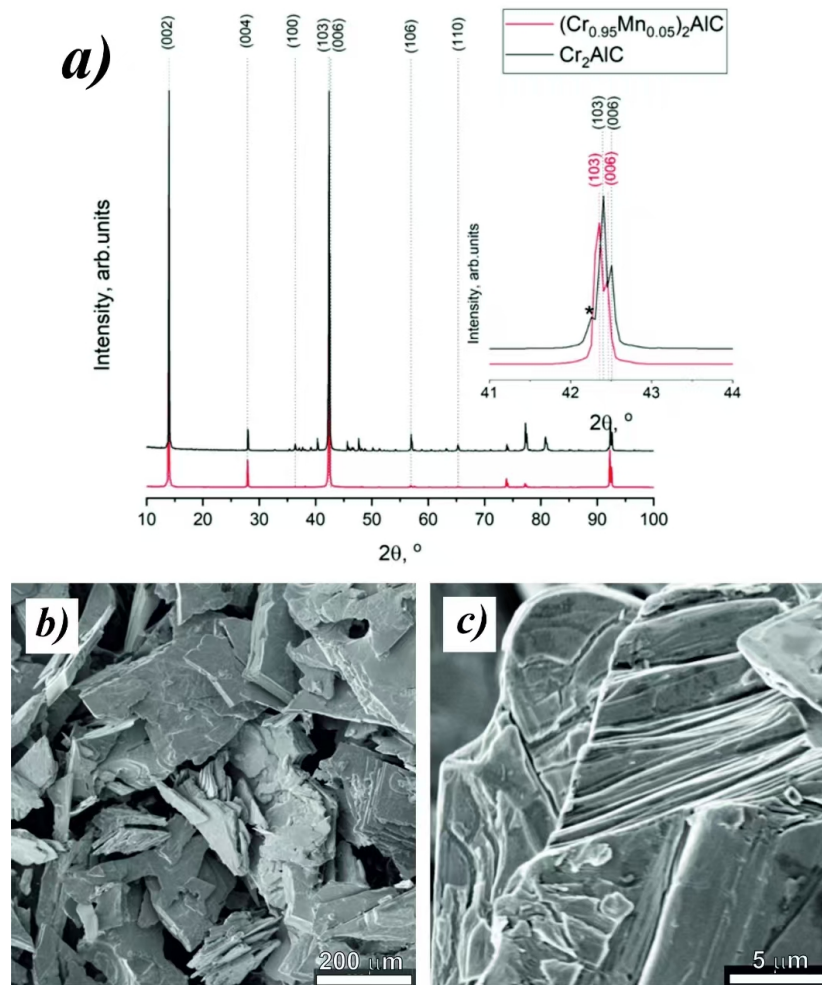


**Fig. 3.** X-ray diffraction spectra of  $(\text{Cr}_{0.95}\text{Mn}_{0.05})_2\text{AlC}$  and  $\text{Cr}_2\text{AlC}$  powders after purification (a) and scanning electron microscopy of powders at various magnifications (b) and (c).

Zhevnenko and Gorshenkov, 2024). Consequently, capillary interaction of MAX-phases with pure copper does not take place, as aluminum forms a two-component melt. However, the introduction of aluminum into the copper-based wetting melt influences the kinetics of the decomposition processes and the release of aluminum from MAX-phases. It is also important to note that for a droplet of pure copper or copper with 17 at.% Al, the wetting line corresponds to the surface of the initial sample, indicating the absence of total dissolution. Fig. 6 illustrates the structure of MAX-phases directly beneath the melt droplet (Fig. 6(a)), at the boundary between the fully decomposed region and the sintered powder of  $(\text{Cr}_{0.95}\text{Mn}_{0.05})_2\text{AlC}$  (Fig. 6(b)), as well as the microstructure of the sintered region (Fig. 6(c)) with corresponding component distribution maps (Figs. 6(d) and 6(e)). These images demonstrate that the use of a copper melt pre-alloyed with aluminum does not completely suppress the decomposition of MAX-phases. However, throughout the entire sample, the powder particles are bonded by a  $\text{Cu}(\text{Al},\text{Cr})$ -based melt.

In general, a higher aluminum content results in an increased concentration of aluminum carbide ( $\text{Al}_4\text{C}_3$ ), which rapidly decomposes in high-humidity environments, even at

room temperature (Park and Lucas, 1997). Consequently, the use of aluminum-based melts is only suitable for systems with high copper content, and soldering processes should be conducted at relatively low temperatures. In contrast, copper-based melts induce the decomposition of MAX-phases in a controlled manner, without causing significant volumetric changes. Further optimization of the alloy composition can be explored within the range of 20-30 at.% Al in Cu to minimize the amount of decomposed MAX-phases while maintaining effective wetting and bonding of the MAX phase powder.

### 3.2 Microhardness of the infiltrated MAX-phases

Exposure to copper at temperatures of 1,084 °C and above results in the formation of a composite material consisting of chromium carbide infiltrated with bronze. A typical microstructure of this composite is shown in the inset of Fig. 7. This transformation leads to a substantial increase in microhardness, nearly by an order of magnitude, from approximately 150  $\text{kg}/\text{mm}^2$  for  $\text{Cr}_2\text{AlC}$  to 1,000-1,300  $\text{kg}/\text{mm}^2$  for the nanostructured region comprising chromium carbides and

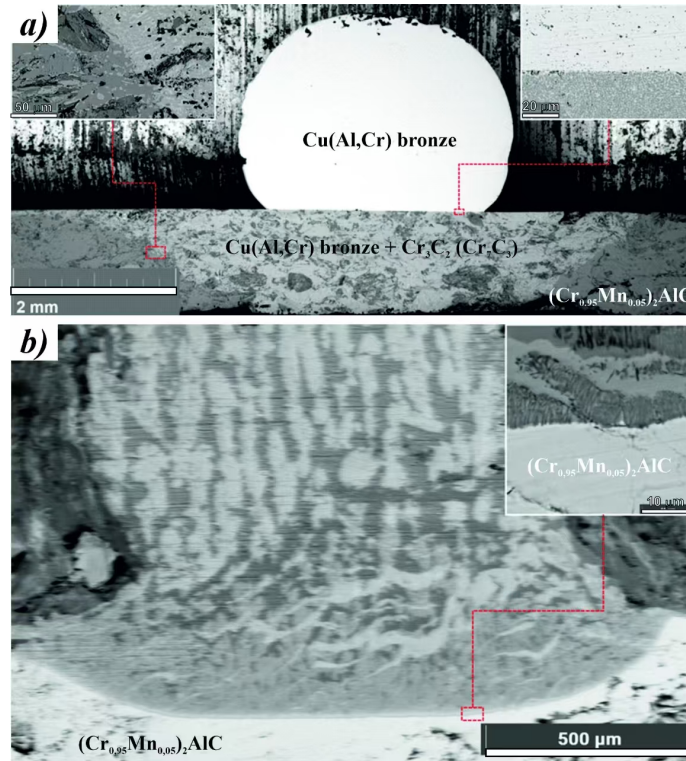


**Fig. 4.** General view and microstructure (inset in the photo) of the contact area between droplets of pure copper (a) and pure aluminum (b) on the surface of  $(Cr_{0.95}Mn_{0.05})_2AlC$  after heating and holding for 60 s at 1,100 °C in vacuum.

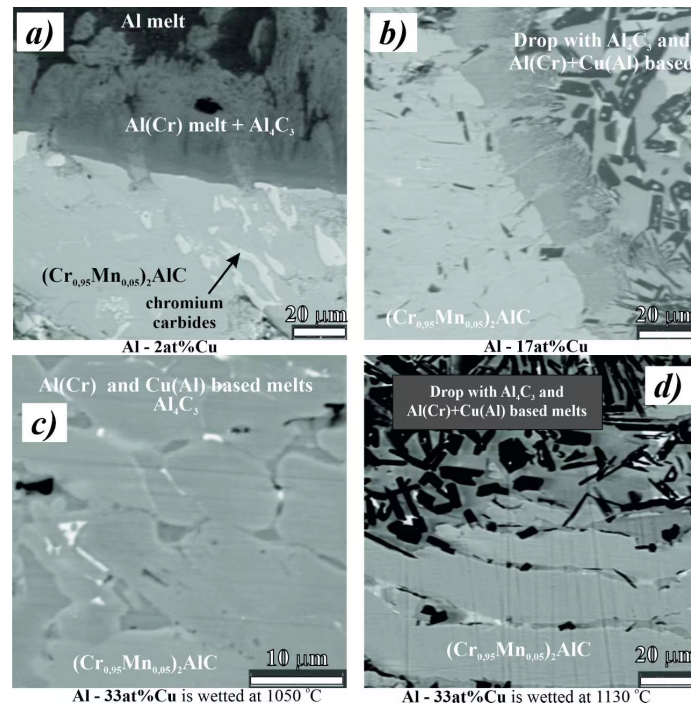


**Fig. 5.** Microstructure of compacted  $(Cr_{0.95}Mn_{0.05})_2AlC$  after heating with droplets of Al-Cu melt: Al+2 at.% Cu (a), Al+17 at.% Cu (b), and Al+33 at.% Cu (c) with holding at 1,050 °C and 1,130 °C (d).

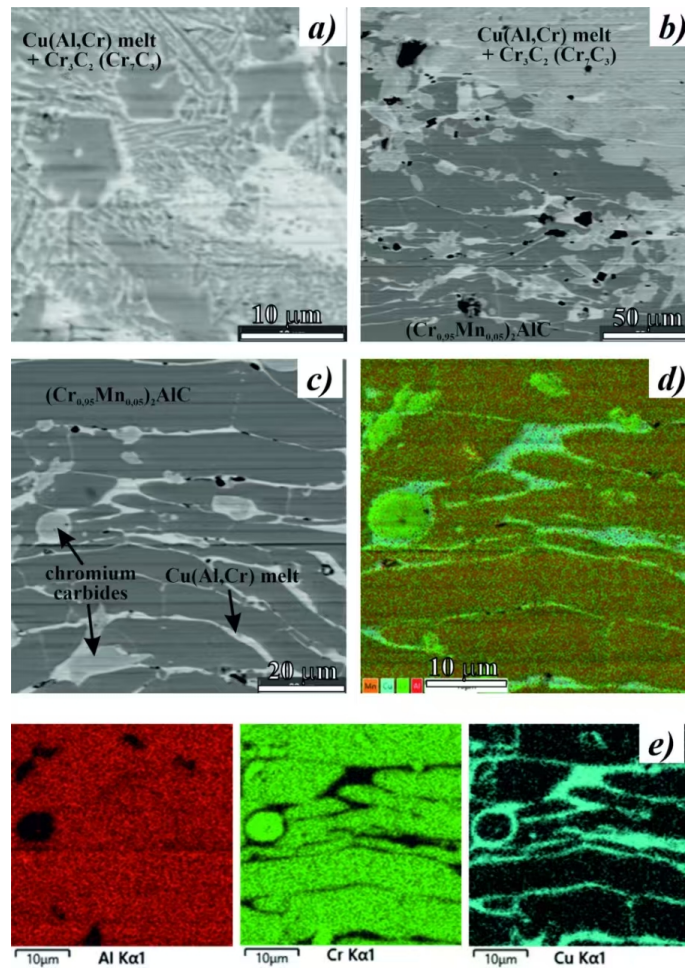


**Fig. 6.** Microstructure of  $(\text{Cr}_{0.95}\text{Mn}_{0.05})_2\text{AlC}$ , interacting with a Cu 17 at%Al melt. a) directly under the melt drop at 1100 °C; b) at the boundary between the fully decomposed region and the bonded powder region, and the microstructure of the bonded region (c) with component distribution maps (d) and (e). The images include color labels corresponding to the elements.

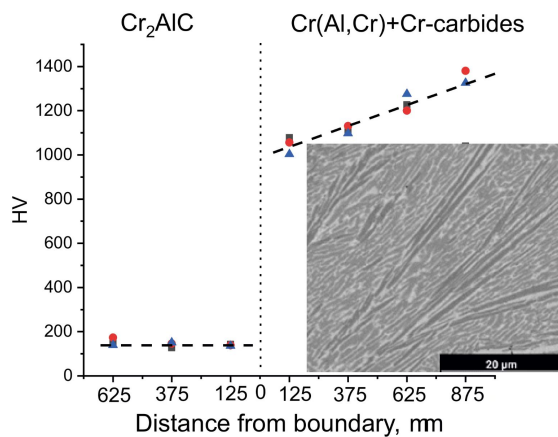


**Fig. 7.** Microhardness of the modified and original areas of sintered  $\text{Cr}_2\text{AlC}$  after exposure to a copper melt. High microhardness corresponds to the decomposed MAX-phases region under the droplet (typical microstructure is shown in inset), and low, to MAX-phases (relative measurement error 15%).

bronze. Fig. 7 presents the Vickers hardness values measured along a line traversing the modified copper droplet region. Neither temperature nor holding time significantly influences the microhardness values of the decomposed region or the sintered  $\text{Cr}_2\text{AlC}$ , as the variations remain within the margin of error. However, the change in the microhardness as a function of distance from the boundary (indicated by the slope of the line in Fig. 7) suggests that the degree of transformation is time-dependent.

The literary data on the microhardness of chromium carbide  $\text{Cr}_3\text{C}_2$  vary over a wide range, most typically from 2,000 kg/mm<sup>2</sup> and above (1,950 kg/mm<sup>2</sup>, 2,755 kg/mm<sup>2</sup>) (Riedel, 2000; Gorshkov et al., 2014). The model describing mechanical properties multiphase composite is the “generalized mixture rule” (Ji, 2004; Ji et al., 2006). In this model, the mechanical properties of composites are expressed as follows:

$$M_C^J = \sum_i^N V_i M_i^J \quad (2)$$

where  $i$  represents the  $i$ -th phase, composites consist of  $N$  phase with volume fraction  $V_i$ , and  $J$  refers to a microstructural exponent that is a scaling, fractal parameter contro-

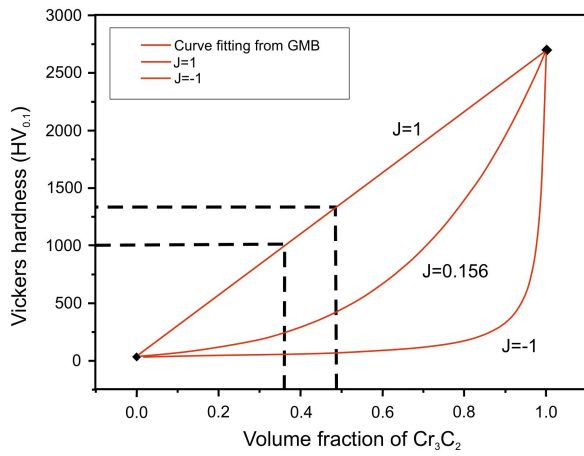


**Fig. 8.** Borrowed from (Zhang et al., 2015). On graph Authors show the microhardness of Cu-Cr<sub>3</sub>C<sub>2</sub> composite (diamonds) and theoretical dependence on generalized mixture rule model at different micro-structural exponents  $J$ . Dotted lines show the relationship between microhardness and volume fraction of the reinforcing phase for  $J = 1$ , which indicates a high degree of hardening efficiency.

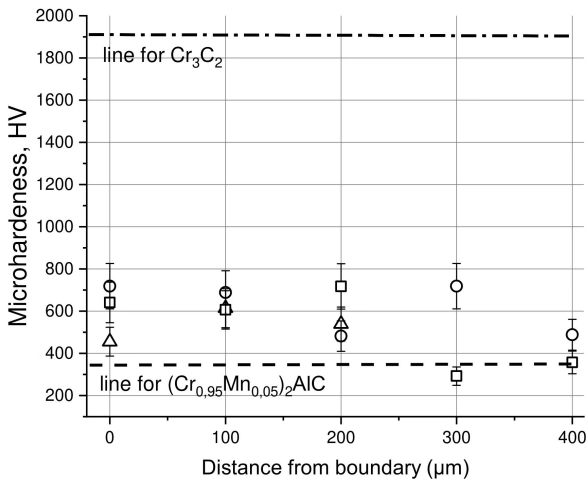


**Fig. 9.** Microhardness of compacted (Cr<sub>0.95</sub>Mn<sub>0.05</sub>)<sub>2</sub>AlC infiltrated with Al+33 at%Cu melt.

lled by the nature of interface boundaries, phases geometry, size distribution, continuity, connectivity etc.. When the composites consist of only two phases, the expression can be simplified as follows:  $M_c^J = V_1 \cdot M_1^J + V_2 \cdot M_2^J$ . When the phases are well-adhered and well-ordered,  $J = 1$ . When the phases are weakly adhered and are irregular in shape,  $J = -1$ . In other cases, the value of  $J$  is between 1 and -1 (except 0) for real materials.

The theoretical density of Cr<sub>2</sub>AlC was selected as 5.24 g/cm<sup>3</sup> (Li et al., 2011), corresponding to a molar volume of approximately 27.3 cm<sup>3</sup>/mol. The molar volume of Cr<sub>2</sub>C was estimated based on the unit cell volume, calculated in (Cao et al., 2022) to be approximately 29 Å<sup>3</sup>/unit cell. By multiplying this value by Avogadro's constant, one can determine the molar volume of Cr<sub>2</sub>C to be 17.5 cm<sup>3</sup>/mol. Consequently, the decomposition of Cr<sub>2</sub>AlC into Cr<sub>2</sub>C and an aluminum melt

results in a porosity of approximately 36%. This porosity is filled with the Cu(Al,Cr) melt, while the remaining volume is occupied by Cr<sub>3</sub>C<sub>2</sub>. Chromium is partially dissolved in the carbides, which deviates from the 2:1 ratio (for Cr<sub>3</sub>C<sub>2</sub>, the ratio is 3:2). Additionally, during the pressing of Cr<sub>2</sub>AlC, a residual porosity of about 20% remains, which is also filled with the melt. As a result, the volume fraction of carbide in the composite is estimated to be approximately 45%-50%. The microhardness of the resulting composite ranges from 1,000 to 1,300 kg/mm<sup>2</sup>, which corresponds to nearly the maximum microstructural coefficient  $J$  (Fig. 8). Fig. 9 presents the microhardness of (Cr<sub>0.95</sub>Mn<sub>0.05</sub>)<sub>2</sub>AlC infiltrated with an Al+33 at.% Cu melt. The microhardness increases by 1.5 to 2 times compared to that of Cr<sub>2</sub>AlC (literature data for the cast MAX-phases with manganese, (Cr<sub>0.95</sub>Mn<sub>0.05</sub>)<sub>2</sub>AlC, are not available). This increase is likely due to a combined effect of manganese-induced strengthening and localized hardening caused by individual particles. The microhardness of aluminum bronze typically ranges from 100 to 300 kg/mm<sup>2</sup> (Rizi and Kokabi, 2014).

### 3.3 Kinetics of Melt interaction with porous MAX-phases

Among the investigated melts, Al+33 at.% Cu exhibits the lowest intensity of MAX-phases dissolution compared to other aluminum-based melts and does not exhibit its decomposition. To study this melt, droplet impregnation experiments were conducted at various temperatures. Typically, infiltration rate measurements are performed by fully immersing a porous sample in the melt or submerging its base. In the Authors' experiments, however, the melt was extruded from a dispenser in the form of a droplet with a diameter ranging from 0.5 to 2 mm. As can be seen in Fig. 4(a), despite the layered structure of the initial MAX-phases powder, the formation of the chemically altered region under the drop occurs in the form of a flattened spheroid. This indicates the isotropy of the movement of chemical components throughout the material as a whole. To evaluate the kinetics of the interaction between the Al+33 at.% Cu melt droplet and the porous (Cr<sub>0.95</sub>Mn<sub>0.05</sub>)<sub>2</sub>AlC substrate (with 20% porosity), a mathematical model of isotropic infiltration for a droplet of finite size was employed. Upon contact with the substrate surface, the droplet assumes a Laplacian shape (Yildiz and Bashiry, 2018) and begins to infiltrate the porous material. In this experimental setup, the diameter of the contact spot ( $d_c$ ) between the melt droplet and the porous substrate surface plays a critical role in characterizing the process (Fig. 10).

Taking into account the finite contact spot diameter factor leads to a non-spherical front of liquid movement through a porous media. Therefore, as a volumetric figure describing the impregnation front, a flattened spheroid, i.e., an ellipsoid, was chosen, which, in Cartesian coordinate system with the axes  $x$  and  $y$ , has major axes  $a$ , and a minor axis  $b$  along the  $z$ -axis (Fig. 11).

The variation in the semi-axes sizes over time can be described as shown in Eqs. (3)-(4):

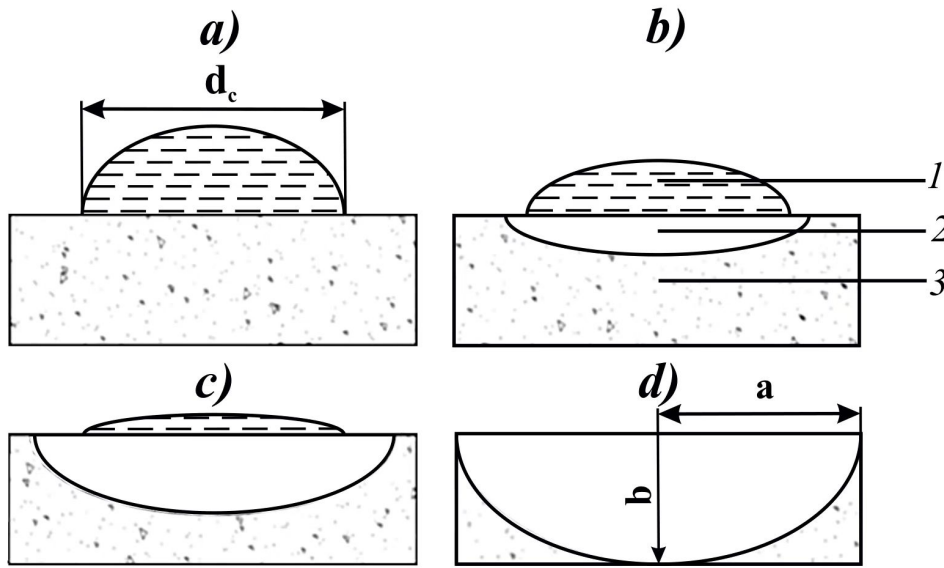


**Fig. 10.** Microstructure of (Infiltration scheme: a-g) sequential stages of infiltration; 1) melt drop, 2) impregnated area of the sample, 3) porous sample; a, b) major and minor axes of the ellipsoid describing the impregnation front.

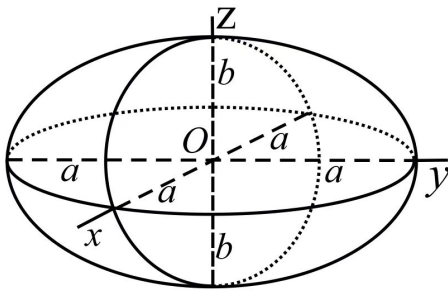


**Fig. 11.** Schematic representation of a flattened spheroid describing the shape of the impregnation front.

$$a(t) = ut + \frac{d_c}{2} \quad (3)$$

$$b(t) = ut \quad (4)$$

where  $u$  is the impregnation front velocity,  $d_c$  is the diameter of the contact spot of the molten droplet with the porous substrate, and  $t$  is time.

By substituting the values of the semi-axes into the formula of the spheroid volume Eq. (5), it is obtained an expression for the dependence of the spheroid volume on time Eq. (6):

$$V_{spd} = \frac{4}{3}\pi a^2 b \quad (5)$$

$$V_{spd}(t) = \frac{4}{3}\pi \left( ut + \frac{d_c}{2} \right)^2 ut = \frac{4}{3}\pi \left( u^3 t^3 + u^2 t^2 d_c + \frac{d_c^2}{4} ut \right) \quad (6)$$

where  $V_{spd}$  is the volume of the spheroid.

Since the impregnation front shape is half of a flattened spheroid, Eq. (6) takes the following form:

$$V_{spd}(t) = \frac{2}{3}\pi \left( u^3 t^3 + u^2 t^2 d_c + \frac{d_c^2}{4} ut \right) \quad (7)$$

The expression for the spheroid volume can be written as follows:

$$V_{spd} = \frac{V_{sp}}{p} \quad (8)$$

where  $V_{sp}$  is the volume of the drop on the surface of the porous substrate,  $p$  is the porosity of the substrate.

As a result, the expression becomes:

$$u^3 + \frac{d_c}{t}u^2 + \frac{d_c^2}{4t^2}u - \frac{3V_{sp}}{2\pi pt^3} = 0 \quad (9)$$

By solving Eq. (9) for the impregnation front velocity, it is possible to obtain the values of the impregnation front velocities.

From Fig. 12, the velocities of the infiltration front were determined at different temperatures: 0.08 mm/s at 1,050 °C and 0.21 mm/s at 1,130 °C. The activation energy of the kinetics at these two points was calculated to be approximately 180 kJ/mol. The observed structural changes and the magnitude of the activation energy suggest that the interaction is chemically driven.

#### 4. Conclusions

This study examined the interaction of Al, Al+2 at.% Cu, Al+17 at.% Cu, Al+33 at.% Cu, Cu+17 at.% Al, and pure copper with porous  $(Cr_{0.95}Mn_{0.05})_2AlC$  and  $Cr_2AlC$  MAX-phases in the temperature range of 1,030–1,100 °C during heating. Despite the large wetting angles (initial contact angles were 130-150°), the melts interact chemically and capillary with the solid phase. It was demonstrated that the transition from pure aluminum to pure copper results in a shift in the nature of the interaction: from the preferential dissolution of MAX-phases in pure aluminum to its decomposition in contact with pure copper, leading to the formation of "bronze-chromium carbide" composite material. High-concentration

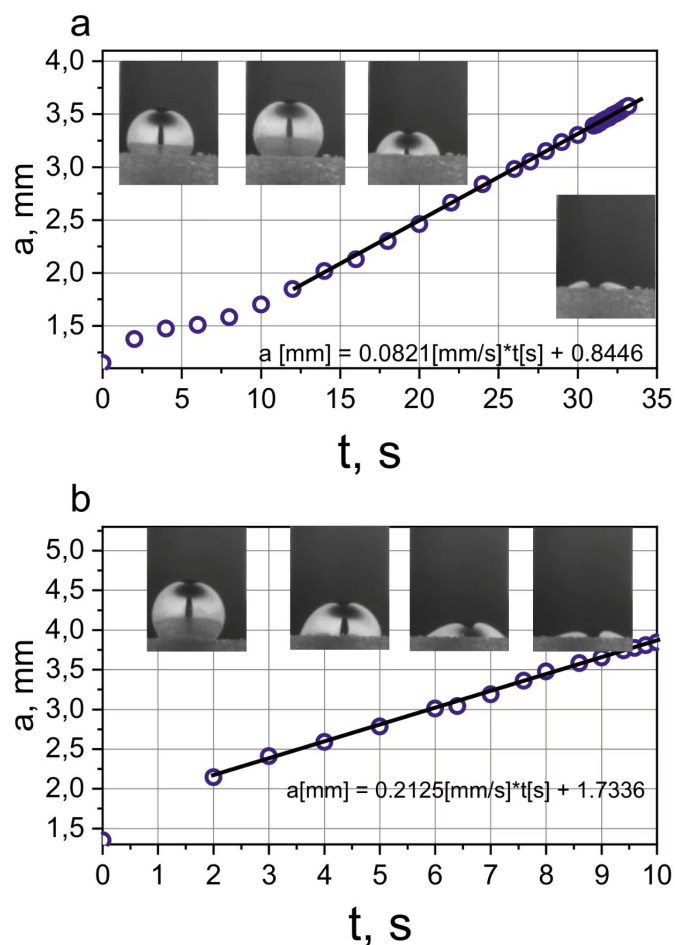


**Fig. 12.** Kinetics of the movement of the Al+30 at.%Cu melt front in  $(Cr_{0.95}Mn_{0.05})_2AlC$  porous media from the melt contact line on the surface at 1,050 °C and 1,130 °C. The tangent of the slope angle corresponds to the velocity of front propagation within MAX-phases. Images of droplets on the surface at various moments of time are provided.

two-component melts, such as Al+17 at.% Cu, Al+33 at.% Cu, and Cu+17 at.% Al, primarily impregnate the porous  $(Cr_{0.95}Mn_{0.05})_2AlC$ , binding the powder particles. Near the contact surface, these melts dissolve MAX-phases, resulting in the formation of aluminum carbide within the melt. The velocity of the Al+33 at.% Cu melt front within the porous  $(Cr_{0.95}Mn_{0.05})_2AlC$  was determined by measuring the change in droplet volume over time at two temperatures: 0.08 mm/s at 1050 °C and 0.21 mm/s at 1,130 °C. Microhardness measurements in the Al+33 at.% Cu-impregnated porous °C and MAX-phases decomposed in contact with the copper melt revealed a slight increase in the mechanical properties in the former case and a significant increase in the hardness in the latter (from approximately 150 kg/mm<sup>2</sup> for  $Cr_2AlC$  to 1,000-1,300 kg/mm<sup>2</sup> for "bronze-chromium carbide" structure). The results of this study provide a basis for recommending the use of Al+33 at.% Cu melt for impregnating  $(Cr_{0.95}Mn_{0.05})_2AlC$  and  $Cr_2AlC$  powders to create composite materials that preserve MAX-phases. Increasing the concentration of aluminum in the melt leads to the formation of a significant amount of aluminum carbide, which destroys the material in an environment containing moisture. Additionally, a method has been

developed for producing a metal matrix composite reinforced with a submicron chromium carbide framework, using MAX-phases as a precursor.

### Acknowledgements

This study was supported by the Russian Science Foundation (No. 23-19-00657).

### Conflict of interest

The authors declare no competing interest.

**Open Access** This article is distributed under the terms and conditions of the Creative Commons Attribution (CC BY-NC-ND) license, which permits unrestricted use, distribution, and reproduction in any medium, provided the original work is properly cited.

### References

Barsoum, M. W., El-Raghy, T. The MAX Phases: Unique new carbide and nitride materials: Ternary ceramics turn out to be surprisingly soft and machinable, yet also heat-tolerant, strong and lightweight. *Journal of the American Ceramic Society*, 2001, 84(2): 424-430.

- Barsoum, M. W., Radovic, M. Elastic and mechanical properties of the MAX phases. *Annual Review of Materials Research*, 2011, 41: 195-227.
- Cao, Q., Liu, S., Li, D. Theoretical studies for stability, mechanical properties, electronic properties, and Debye temperature of novel Cr<sub>2</sub>C structures. *Journal of Materials Science*, 2022, 57(40): 18969-18979.
- Gonzalez-Julian, J., Onrubia, S., Bram, M., et al. Effect of sintering method on the microstructure of pure Cr<sub>2</sub>AlC MAX phase ceramics. *Journal of the Ceramic Society of Japan*, 2016, 124(4): 415-420.
- Gorshkov, V. A., Kachin, A. P., Yukhvid, V. I. SHS-metallurgy of cast Cr<sub>3</sub>C<sub>2</sub>-NiAl composites and protective coatings on its base. *Perspektivnye Materialy*, 2014, 10: 60-66.
- Gorshkov, V. A., Miloserdov, P. A., Khomenko, N. Y., et al. High-temperature synthesis of composite materials based on (Cr,Mn,V)-Al-C MAX phases. *Ceramics International*, 2021, 47(18): 25821-25825.
- Gorshkov, V. A., Miloserdov, P. A., Sachkova, N. V., et al. SHS metallurgy of Cr<sub>2</sub>AlC MAX phase-based cast materials. *Russian Journal of Non-Ferrous Metals*, 2018, 59(5): 570-575.
- Ji, S. C. Generalized means as an approach for predicting Young's moduli of multiphase materials. *Materials Science and Engineering: A*, 2004, 366: 195-201.
- Ji, S. C., Gu, Q., Xia, B. Porosity dependence of mechanical properties of solid materials. *Journal of Materials Science*, 2006, 41: 1757-1768.
- Kennedy, A. R., Wood, J. D., Weager, B. M. The wetting and spontaneous infiltration of ceramics by molten copper. *Journal of Materials Science*, 2000, 35: 2909-2912.
- Lei, X., Lin, N. Structure and synthesis of MAX phase materials: A brief review. *Critical Reviews in Solid State and Materials Sciences*, 2022, 47(5): 736-771.
- Li, H., Li, S., Zhou, Y. Cyclic thermal shock behavior of a Cr<sub>2</sub>AlC ceramic. *Materials Science and Engineering: A*, 2014, 607: 525-529.
- Li, J., Jing, J., He, J., et al. Microstructure evolution and elemental diffusion behavior near the interface of Cr<sub>2</sub>AlC and single crystal superalloy DD5 at elevated temperatures. *Materials and Design*, 2020, 193: 108776.
- Li, S. B., Yu, W. B., Zhai, H. X., et al. Mechanical properties of low-temperature synthesized dense and fine-grained Cr<sub>2</sub>AlC ceramics. *Journal of the European Ceramic Society*, 2011, 31(1-2): 217-224.
- Liu, X. J., Ohnuma, I., Wang, C. P., et al. Thermodynamic database on microsolders and copper-based alloy systems. *Journal of electronic materials*, 2003, 32: 1265-1272.
- Mockute, A., Dahlqvist, M., Emmerlich, J., et al. Synthesis and ab initio calculations of nanolaminated (Cr,Mn)<sub>2</sub>AlC compounds. *Physical Review B*, 2013, 87(9): 094113.
- Park, J. K., Lucas, J. P. Moisture effect on SiCp/6061 Al MMC: Dissolution of interfacial Al<sub>4</sub>C<sub>3</sub>. *Scripta Materialia*, 1997, 37(4): 511-516.
- Pittoni, P. G., Chang, Y. -Y., Lin, S. -Y. The effect of interfacial morphology on wetting of graphite by molten silver at high temperature. *Journal of Materials Science*, 2012, 47: 8395-8403.
- Riedel, R. *Handbook of Ceramic Hard Materials*. Wiley-VCH Verlag GmbH, Weinheim, Germany, 2000.
- Rizi, M. S., Kokabi, A. H. Microstructure evolution and microhardness of friction stir welded cast aluminum bronze. *Journal of Materials Processing Technology*, 2014, 214(8): 1524-1529.
- Sarina, B. A. O., Tang, K., Kvithyld, A., et al. Wetting of pure aluminium on graphite, SiC, and Al<sub>2</sub>O<sub>3</sub> in aluminium filtration. *Transactions of Nonferrous Metals Society of China*, 2012, 22(8): 1930-1938.
- Shamsipoor, A., Farvizi, M., Razavi, M., et al. Influences of processing parameters on the microstructure and wear performance of Cr<sub>2</sub>AlC MAX phase prepared by spark plasma sintering method. *Journal of Alloys and Compounds*, 2020, 815: 152345.
- Smialek, J.L., Garg, A. Interfacial reactions of a MAX phase/superalloy hybrid. *Surface and Interface Analysis*, 2015, 47: 844.
- Sokol, M., Natu, V., Kota, S., et al. On the chemical diversity of the MAX phases. *Trends in Chemistry*, 2019, 1(2): 210-223.
- Tabares, E., Kitzmantel, M., Neubauer, E., et al. Sinterability, mechanical properties, and wear behavior of Ti<sub>3</sub>SiC<sub>2</sub> and Cr<sub>2</sub>AlC MAX phases. *Ceramics*, 2022, 5(1): 55-74.
- Wang, Y., Xu, D., Yan, H., et al. Low-temperature copper sinter-joining technology for power electronics packaging: A review. *Journal of Materials Processing Technology*, 2024, 118526.
- Yildiz, B., Bashiry, V. Shape analysis of a sessile drop on a flat solid surface. *The Journal of Adhesion*, 2018, 95: 929-942.
- Zakeri-Shahroudi, F., Ghasemi, B., Abdolahpour, H., et al. Sintering behavior of Cr<sub>2</sub>AlC MAX phase synthesized by spark plasma sintering. *International Journal of Applied Ceramic Technology*, 2022, 19(3): 1309-1318.
- Zhang, L., Pang, X., Gao, K., et al. Mechanical properties of a bi-continuous Cu-Cr<sub>3</sub>C<sub>2</sub> composite. *Materials Science and Engineering: A*, 2015, 623: 4-9.
- Zhevnenko, S. N., Gorshenkov, M. V. Wetting and spreading of Cu(Cr) melt over the Cr<sub>2</sub>AlC MAX phase. *Materials Letters*, 2022, 324: 132711.
- Zhevnenko, S. N., Gorshenkov, M. V. Capillary phenomena during interaction of copper melt with dense and porous MAX phases with general formula (Cr, Mn)<sub>2</sub>AlC. *Physics of Metals and Metallography*, 2024, 125(2): 156-165.
- Zuber, A., Gauthier-Brunet V., Dubois, S. Cr<sub>2</sub>AlC and metals reactivity: Sintering and oxidation. *Open Ceramics*, 2024, 17: 100561.